Steel and Composite Structures, *Vol. 14, No. 6 (2013) 547-569*
DOI: http://dx.doi.org/10.12989/scs.2013.14.6.547

Hysteretic behavior of dissipative welded fuses for earthquake resistant composite steel and concrete frames

Luís Calado*[1], Jorge M. Proença[1a], Miguel Espinha[1] and Carlo A. Castiglioni[2]

[1]*Department of Civil Engineering and Architecture, Instituto Superior Técnico, Technical University of Lisbon, Av. Rovisco Pais 1, 1049-001 Lisbon, Portugal*
[2]*Structural Engineering Department, Politecnico di Milano, Piazza L. da Vinci, 32 - 20133 Milan, Italy*

(Received April 23, 2011, Revised March 28, 2013, Accepted May 20, 2013)

Abstract. In recent years there has been increasing international interest about designing structures that cost less to repair after they have been subjected to strong earthquakes. Considering this interest, an innovative repairable fuse device has been developed for dissipative beam-to-column connections in moment-resisting composite steel and concrete frames. The seismic performance of the device was assessed through an extensive experimental program comprising ten cyclic and two monotonic tests. These tests were conducted on a single beam-to-column specimen with different fuse devices for each test. The devices varied in terms of the chosen geometric and mechanical parameters. The tests showed that the devices were able to concentrate plasticity and to dissipate large amounts of energy through non-linear behavior. Numerical models were developed with Abaqus and simplified design models are also proposed.

Keywords: welded fuse device; reparability; cyclic tests; hysteretic behavior; plate buckling; energy dissipation; numerical models; design models

1. Introduction

Seismic events in Northridge (USA 1994) and Kobe (Japan 1995) led to widespread failure of a large number of beam-to-column connections in moment-resisting steel frames (Engelhardt and Sabol 1997). With the appearance of seismic-resistant technologies societies in developed countries have become more demanding in terms of the seismic performance of modern structures. In order to deal with these strict requirements that go further than safety, recent advances have been directed towards achieving high performance standards in terms of economic and sustainable construction. In seismic areas this trend results in increasing concerns with the reparability of structures damaged by strong earthquakes.

In the last few years new design approaches have been implemented that aim at shifting the plastic hinge and the associated large plastic deformations into the beams, away from the potentially brittle beam-to-column connection welds, avoiding also that damage extends to the beam-column node (panel zone). Among the preferred solutions are those that introduce weakened

*Corresponding author, Full Professor, E-mail: calado@civil.ist.utl.pt
[a] Associate Professor, E-mail: jorge.m.proenca@ist.utl.pt

http://www.techno-press.org/?journal=scs&subpage=8 ISSN: 1229-9367 (Print), 1598-6233 (Online)

areas near the beam ends that are able to concentrate plasticity and develop large deformations and, thus, force the location of the plastic hinges (Mazzolani 2000).

One of the first solutions of this type was the reduced beam section (RBS), introduced by Plumier (1990). This solution, despite being able to successfully dissipate energy and concentrate plasticity, as shown experimentally (Pachoumis *et al*. 2010, Yu and Uang 2001), presented difficulties in terms of the reparability of damaged parts of the structure. New solutions are now indicating devices that can simultaneously dissipate energy through the non-linear behavior of their components and be easily repaired. Significant developments have been achieved in research on dissipative and easy-replaceable fuses for eccentrically braced frames (EBF), concentrically braced frames (CBF) and knee braced frames (KBF). Chan *et al*. (2009), Li and Li (2007) and Bruneau *et al*. (2010) conducted experimental tests on EBF systems with different link geometries. Plumier *et al*. (2004) developed innovative dissipative systems for CBF that comprised pinned and "U" type connections. The dissipative capacities of KBF systems were studied by Hsu and Chou (2011), who performed cyclic experimental tests on a frame with different knee brace geometries.

Focusing on moment resisting frames (MRF), experimental cyclic tests have been widely used to investigate the dissipative capacities of traditional bolted and welded moment connections (Dubina *et al*. 2002, Adany *et al*. 2001, Mele *et al*. 2001). Koetaka *et al*. (2005) proposed alternative weld-free moment connections between composite steel-concrete beams and the weak axis of the column. These connections are made through replaceable steel plates bolted to the upper and lower flanges of the beam. Oh *et al*. (2009) developed an innovative fuse based on a damper system fitted at the bottom flange of the beam at the beam-to-column connection.

This scenario is what motivated the FUSEIS project research of its aim is to develop innovative fuse devices for moment-resisting composite steel and concrete frames, with the following functional objectives: devices that are easy to design and produce/assemble; high seismic performance and low-cost repair work. Given these objectives, preliminary numerical investigations were undertaken by Mazza and Pedrazzoli (2008), which concluded with the optimal fuse configurations, resulting in one bolted and one welded solutions. The work described in this paper focuses on the experimental and numerical investigations on the welded fuse alternative (the bolted alternative is presented in another paper by Castiglioni *et al*. (2012)).

2. Experimental program

2.1 Fuse specimens

The basic test assembly consisted of a typical beam-to-column sub-assemblage, comprising a composite beam with an IPE300 profile supporting a 150 mm thick and 1450 mm wide reinforced concrete slab, with a HEB240 profile column, as shown in Fig. 1.

The fuse device studied consists of steel plates welded to the web and bottom flange of the beam, together with a specifically detailed slab gap, as schematically shown in Fig. 1. Non-linear behavior should be concentrated only in the fuse plates, which can easily be replaced by unwelding the damaged plates and welding the new ones. Post-earthquake damage inspection should be directed to the detection of residual rotation at the fuse (considered a sign of general fuse damage) or more localized damage symptoms in the replaceable parts, such as (web or flange) plate buckling.

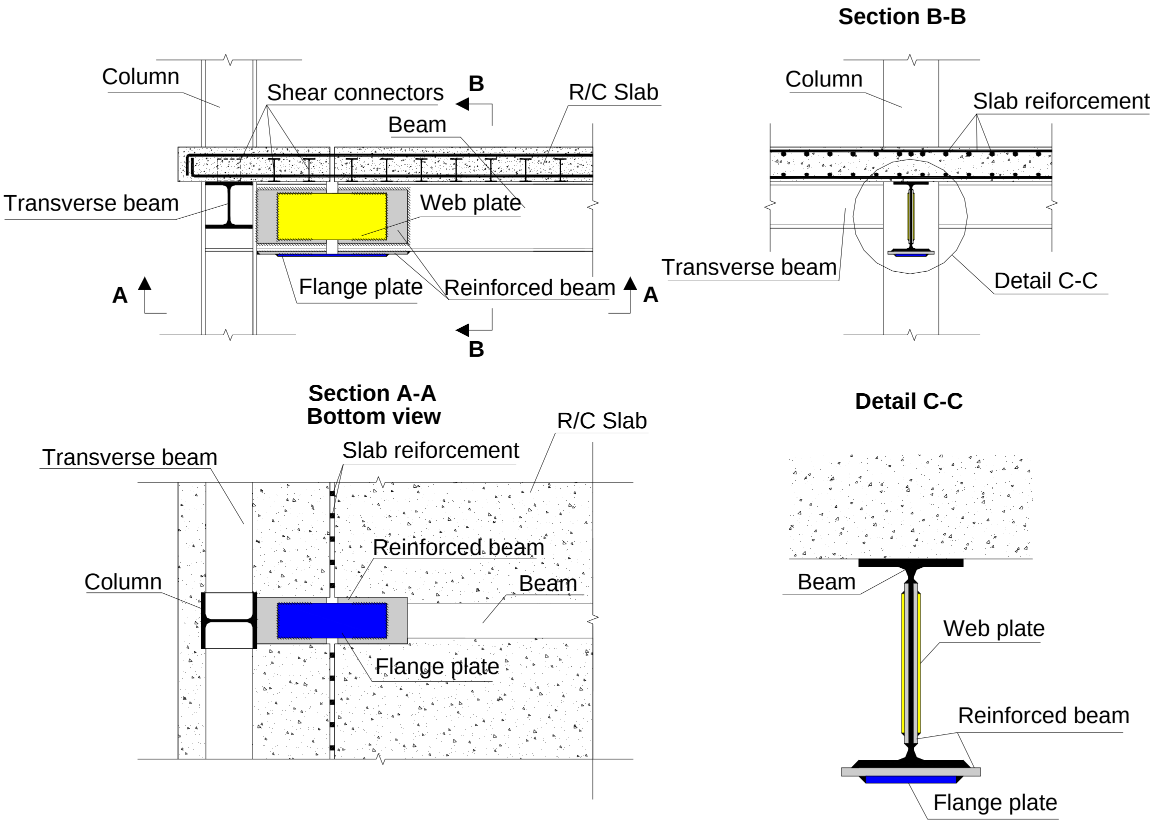

Fig. 1 Scheme of the welded fuse device

The gap under the slab, just over the fuse, was intended to avoid major damage to the concrete by allowing the fuse to develop large rotations. The gap width in the reinforced concrete part of the fuse could be different from that of the steel parts of the fuse. The recommended values for the gap width in the reinforced concrete (slab) and in the steel parts are, respectively, 10% of the height of the slab and 10% of the total height of the composite cross-section. The longitudinal rebars are continuous over the gap, thus ensuring transmission of stresses. Considering that the rebars are irreplaceable, their yielding is prevented by forcing both the elastic and plastic neutral axes to lie within the concrete slab thickness. To achieve this result the total area of the rebars was always more than twice of that of the flange plate. The longitudinal reinforcement of the slab (thickness 150mm) consisted in ϕ20/100, top layer, and ϕ16/100 + ϕ12/200, bottom layer (dimensions in mm). Although not mandatory for the fuse concept under study, the tested specimens were manufactured with flexible (also termed ductile) connectors designed for full connection capacity. The reinforced beam zone is an area reinforced with additional welded plates and is intended to avoid plasticity spreading to the adjacent irreplaceable steel parts of the beam and also to protect the beam surface from damage caused by repeated welding and unwelding. There are no definite design indications for these reinforcement plates but the tested specimens were fitted with reinforcement plates with cross sectional areas roughly equivalent to those of the corresponding parts of the steel profile (web or flange).

Table 1 Dimensions of the flange plates of the fuses (in mm) and geometric slenderness

Plate	A	B	C	D	E	F
t_f	10	10	12	8	12	8
b_f	80	130	110	100	150	140
λ_G	17.0	17.0	14.2	21.3	14.2	21.3

To assess the performance of the fuse device a total of ten cyclic and two monotonic experimental tests were conducted on a single sub-assembly of a beam-to-column connection fitted with fuses with different geometric parameters.

Each test was conducted until complete failure of the fuse flange plate, after which the fuse plates were replaced by new ones and another test was performed. The web plates were designed to withstand shear forces and had the same dimensions in all tests. The only dimensions that changed between tests, therefore, were the thickness (t_f) and width (b_f) of the flange plates, since the free buckling length L_0 of the steel plates was 170 mm for all specimens. The free buckling length was not varied so that, through variations of the thickness and width of the steel plates the effects of buckling and capacity ratio could be studied as separately as possible. The buckling susceptibility was described by the geometric slenderness λ_G, computed as the ratio between free length and thickness of the flange plates. L_0 was set constant so that the tensile strain imposed in the flange plates for the intended fuse rotation amplitudes could adequately be placed in the plastic range, yet far from that of tensile fracture for monotonic tests.

The dimensions presented in Table 1 were chosen to provide the fuses with different values of a controlling design parameter, the *capacity ratio* α, defined by Eq. (1)

$$\alpha = \frac{M_{\max,fuse}}{M_{pl,beam}} \tag{1}$$

where $M_{\max,fuse}$ is the maximum moment developed by the fuse device and $M_{pl,beam}$ is the plastic resisting moment of the non-reinforced segment of the composite cross-section of the beam (away from the fuse, without the web and flange reinforcing plates).

The maximum moments of the fuse $M_{\max,fuse}$ were computed with a design model developed by Espinha (2011), which is described in Section 5. The corresponding values of the capacity ratio are presented in Table 2 for both sagging (α^+) and hogging (α^-) moments.

It should be noted that the hogging capacity ratio α^- takes into account the buckling phenomenon of the steel parts, which depends on the slenderness of the fuse plates. As shown previously, the geometric slenderness parameter λ_G varied between 14.2 (fuse plates C and E) and 21.3 (fuse plates D and F).

Table 2 Capacity ratios of the fuses

Plate	A	B	C	D	E	F
α^+	0.45	0.57	0.57	0.47	0.71	0.54
α^-	0.27	0.38	0.39	0.25	0.48	0.30

Testing was conducted in three main phases – first, cyclic, for plates D, A, B and C, in that order, with repetitions – and afterwards, cyclic, for a new set of plates – F and E, in that order – and in the end, monotonic, sagging and hogging, for plate C. The testing sequence was devised to reduce the effects of accumulated damage induced by previous tests, i.e., in the order of increasing strength (capacity ratio) and, in cases of equivalent strength, decreasing geometric slenderness. The majority of the tests were conducted with plates A to D; plates E and F were tested afterwards to allow a finer description of the influence of the capacity ratio (shown in previous tests to be one of the most influential design variables); the monotonic test was conducted with specimen C, corresponding to an intermediate capacity ratio.

2.2 Experimental set-up and loading history

The experimental test set-up is shown schematically in Fig. 2.

Apart from the controlling transducers – top displacement and force, depicted in Fig. 2 – the tested specimens were instrumented with a series of 21 more displacement transducers, shown in Fig. 3, to monitor the rigid body motion at the supports, the rotations and transversal displacements at different positions along the beam length and the beam-to-slab slip.

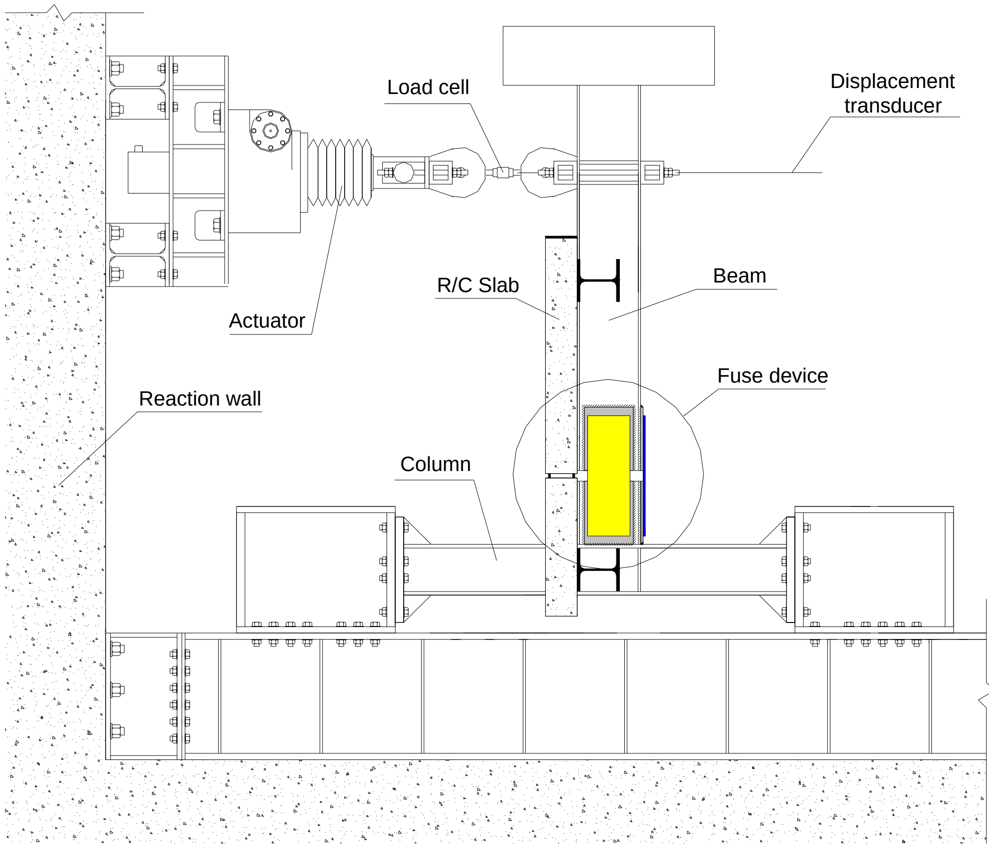

Fig. 2 Experimental test set-up

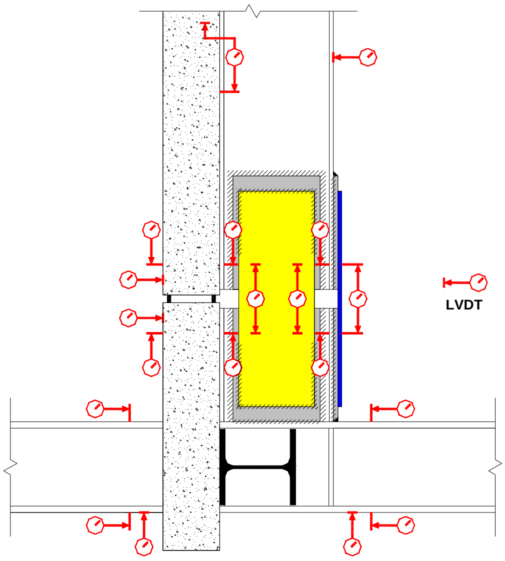

Fig. 3 Location of remaining LVDTs (close-up)

Table 3 Loading history protocol

Step (n)	Imposed top displacement (mm)	Approximate device rotation θ (mrad)	Nr. of cycles
1	2.25	1.5	3
$2 \leq n \leq 5$	3.75 (n-1)	2.5 (n-1)	3
$6 \leq n \leq 11$	7.50 (n-3)	5.0 (n-3)	3
$n > 11$	60	40	3

The cyclic displacements are imposed on the specimen by the actuator at the top of the beam, at a vertical distance of approximately 1.5 m from the center of the fuse device. The loading history was based on a protocol similar to the one proposed in the ECCS Recommendations (1986), translated in terms of the approximate device rotation, which is independent of the yield displacement, as suggested by Krawinkler (2009). The loading history protocol is described in Table 3 in terms of the step index n. If failure had not been reached after completing the eleven steps of the proposed loading history, cycles with 40 mrad device rotation amplitude (60 mm) would have been performed until complete failure of the flange plate.

3. Analysis of the experimental results

3.1 Overall hysteretic behavior

The analysis of the results was mainly based on the moment-rotation in the fuse ($M - \theta$) diagrams of the specimens. As an example, the $M - \theta$ diagrams for both tests on fuse D are shown in Fig. 4 (rotation θ is approximately computed dividing the top displacement by the distance to the center of the fuse).

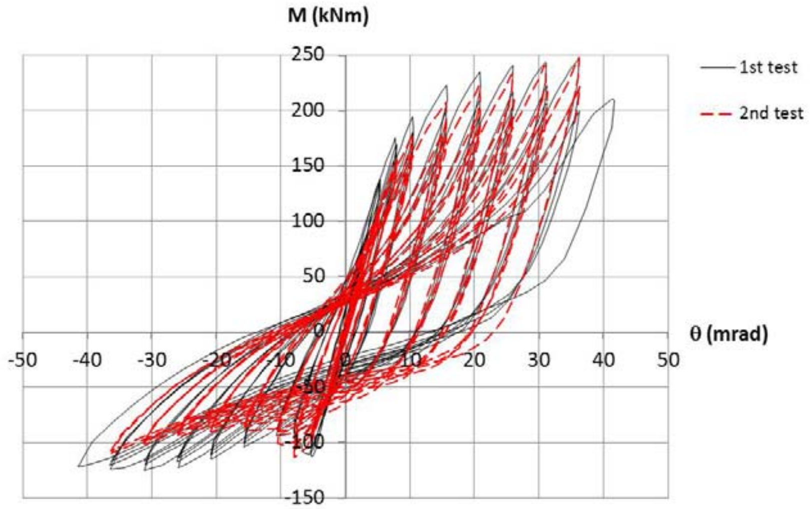

Fig. 4 $M-\theta$ diagram of plate D

(a) (b)

Fig. 5 Typical failure modes of the flange plate of the fuse

The diagrams show that the hysteretic behavior of the fuses is stable, characterized by a marked pinching phenomenon due to the buckling of the fuse plates when under hogging rotation, which also explains the asymmetry of the diagram in terms of moments. The deformation capability of the fuses is demonstrated by the fact that all specimens were able to perform ± 35 mrad rotations, which is the minimum recommended by EN 1998-1 (CEN 2004). Moreover, apart from the second tests on specimens A, C and D, all other fuses achieved rotations in excess of ± 41 mrad.

Comparison of the $M-\theta$ diagrams between the first and second tests of the same fuse specimen shows that there is a slight deterioration in terms of strength and energy dissipation. This deterioration is a consequence of the accumulated damage to the parts of the test assembly that are not replaced between tests.

The failure modes of all cyclically tested specimens were identical and consisted of the

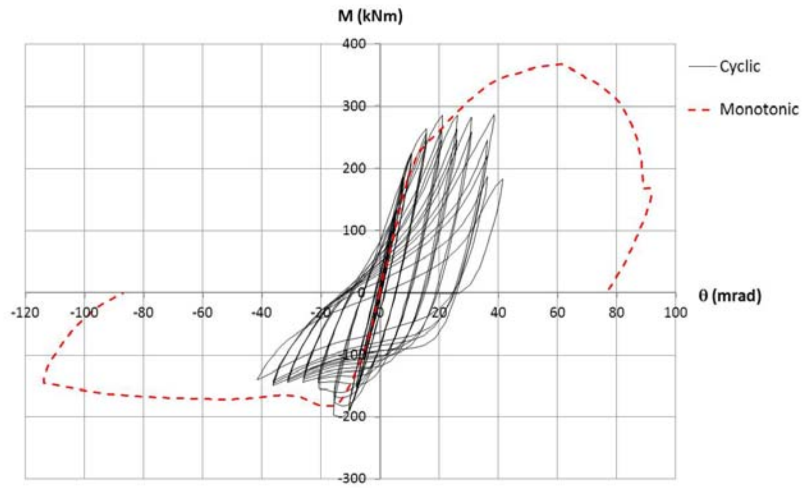

Fig. 6 Comparison between monotonic and cyclic tests conducted on fuse C

development of cracks at the mid-section of the flange plate under tension, as shown in Figs. 5(a)-(b).

The monotonic sagging test was stopped before failure due to fuse closure (contact between the adjoining beam flanges) for approximate fuse rotation of nearly 120 mrad.

Measurements showed that both the column and the composite beam remained in the elastic range, moving in a manner similar to rigid bodies with little elastic deformation. The specimens showed a significant composite behavior, with slip at the slab-beam interface proving to be relatively small, with values below 0.20 mm for all specimens.

The monotonic behavior can be compared with the cyclic behavior by superimposing the corresponding $M - \theta$ diagrams, as shown in Fig. 6 for the plate C fuse.

The diagrams are similar in terms of the initial stiffness and yield moments. The monotonic diagram seems to fit well with the cyclic diagram for the same rotation range, closely resembling the cyclic envelope curve. The combination of kinematic strain hardening (which increases monotonic strength) with low cycle fatigue (which decreases cyclic strength) justifies the strength differences observed in the sagging direction. Strength in the hogging direction is controlled by the buckling phenomenon which occurs irrespective of the fact that the tests are monotonic or cyclic. The deformation capacity of the cyclic tests is considerably reduced due to damage accumulation effects (e.g., low cycle fatigue of the flange plate).

The performance of the fuses was subsequently evaluated considering primarily the stiffness, strength and energy dissipation.

3.2 Stiffness

Fig. 7 shows the stiffness at the end of each cycle in terms of the variation of the ξ parameter, defined in the ECCS Recommendations (1986) as being the ratio between the unloading stiffness at the end of each of cycle and the initial elastic stiffness of the specimen.

The results presented in the diagram refer to the first test on each of the fuse plates. The

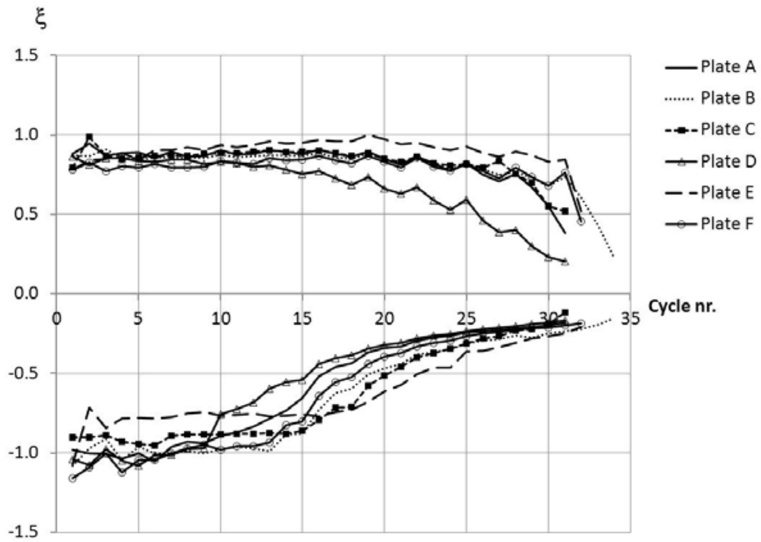

Fig. 7 Stiffness ratio at the end of each cycle

diagram enables us to state that, in general, the curves show a similar trend with respect to the cycle number for all specimens for both sagging and hogging rotations. As expected, there is a stiffness loss with cycling, which leads to the progressive decrease of the ξ parameter to values below unity ($\xi = 1$, elastic stiffness).

When sagging and hogging behavior are compared it becomes clear that a more expressive stiffness loss occurs under hogging, which could be explained by the stiffness loss induced by cyclic buckling of the fuse plates. Comparison of the curves for plates with low and high values of α (e.g., plates D and E, respectively) shows that specimens with lower values of α also lose stiffness at a faster rate with cycling, especially under sagging rotation.

3.3 Strength

In order to simplify the test comparisons, the dimensionless resistance ratio ε at the end of each cycle is presented in Fig. 8 for the first test of each specimen. This ratio is defined in ECCS (1986) as the bending moment at the end of each cycle divided by the yield moment of the specimen in the corresponding direction.

The trend of the resistance ratio with cycling seems to be very similar for all specimens in sagging rotation, presenting a considerable hardening, which in some cases reaches a value of 1.5 times the yield moment. This phenomenon is mainly due to the hardening of the flange plate in tension, which is explained by the marked hardening also found in tensile tests of mild steel specimens. However, for hogging rotation, the aforementioned strain hardening effects are balanced by those attributable to buckling, also in the flange plates, so that the resistance ratio is generally lower than unity.

The sagging and hogging resistance of the fuses are expected to be directly controlled by the values of the capacity ratios α^+ and α^-, respectively. This dependence is shown in the charts in Figs. 9 and 10.

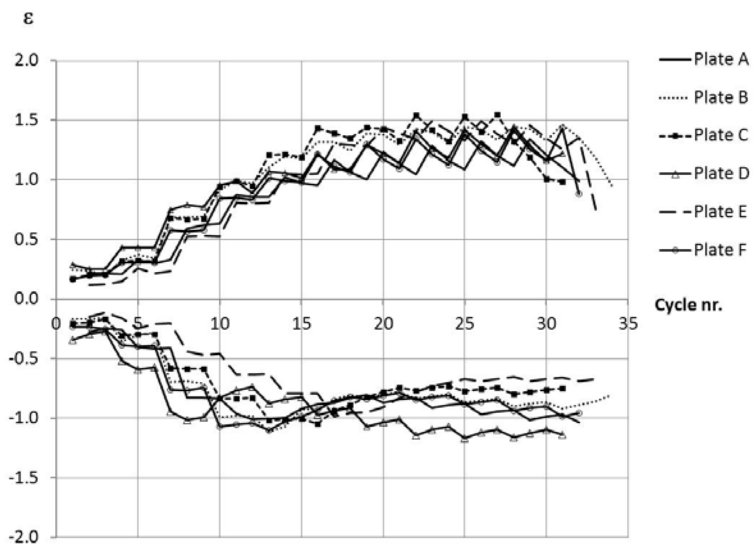

Fig. 8 Resistance ratio at the end of each cycle

The sagging resistance chart in Fig. 9 shows that both yield (My) and maximum moments (*M*max), both determined according to ECCS Recommendations (1986), increase with α^+, showing a reasonable correlation. Nevertheless there are some exceptions, where the same value of α^+ corresponds to different values of resistance. This apparently contradictory behavior was observed in the specimens that were tested last, where the damage accumulation effects from previous tests led to resistance losses, which are disregarded in the computation of α.

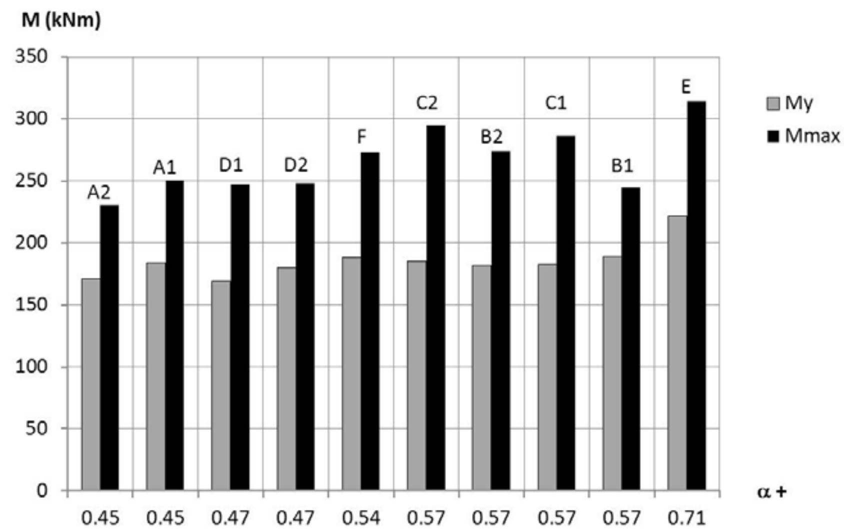

Fig. 9 Sagging resistance vs. α^+

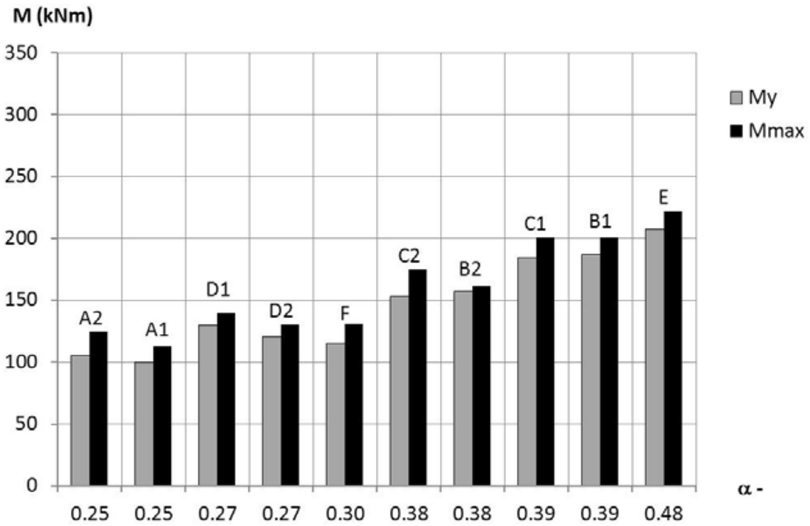

Fig. 10 Hogging resistance vs. α^{-}

As for the hogging moments, Fig. 10 shows that strength exhibits a more consistent increase with the capacity ratio. This shows that the hogging resistance of the fuse might be more sensitive to a geometry variation of the flange plate and consequently of α^{-}.

3.4 Energy dissipation

Energy dissipation capacity plays one of the most important roles in describing the seismic performance of the fuses. The total amount of dissipated energy W_{total} was computed for each test and the variation with respect to the value of α^{+} is shown in Fig. 11.

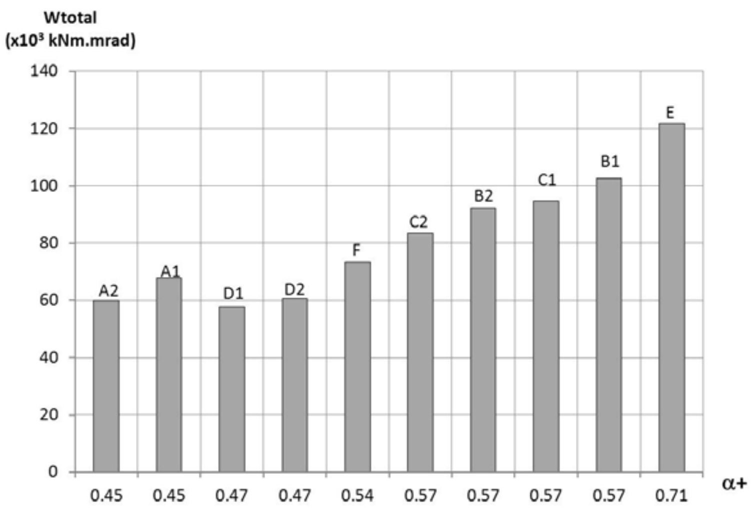

Fig. 11 Total amount of dissipated energy vs. α^{+}

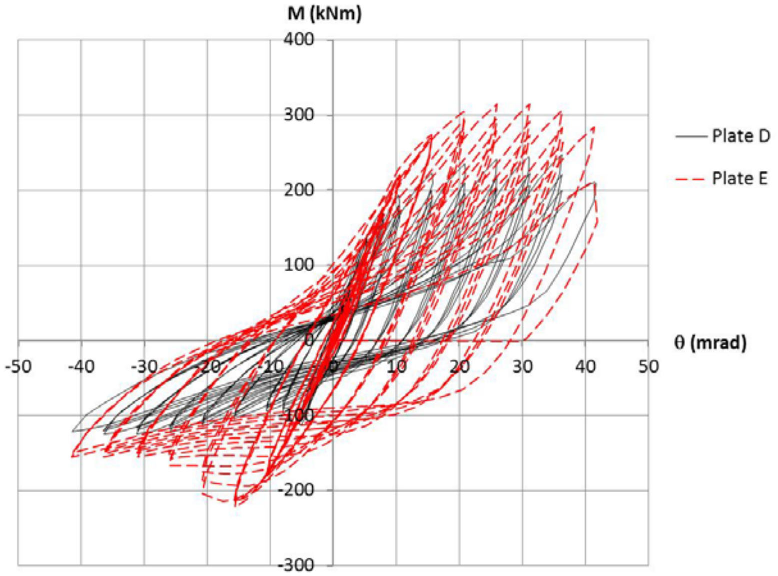

Fig. 12 Comparison between moment-rotation diagrams of plates D and E

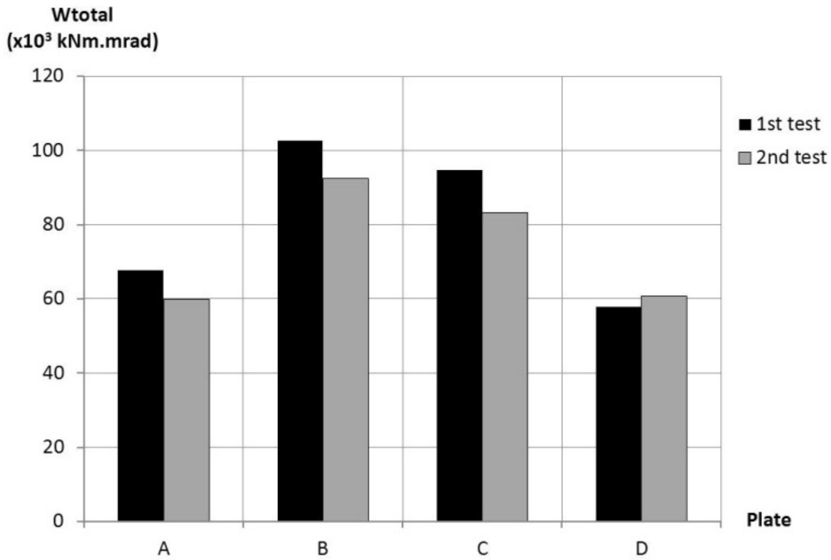

Fig. 13 Comparison between first and second tests in terms of energy dissipation

The correlation shown by the chart in Fig. 11 leads to the conclusion that the α^+ parameter seems to be able to translate the influence of the capacity of the fuse on the energy dissipation capacity of the specimen, but it is stressed that the severity of the yielding and buckling of the fuse parts have a fundamental influence on the performance of the fuse. This aspect may also be recognized by observing the shapes of the moment-rotation diagrams. Fig. 12 clearly shows the difference between plates with extreme values of α^+ (i.e., plates D and E), mainly due to the

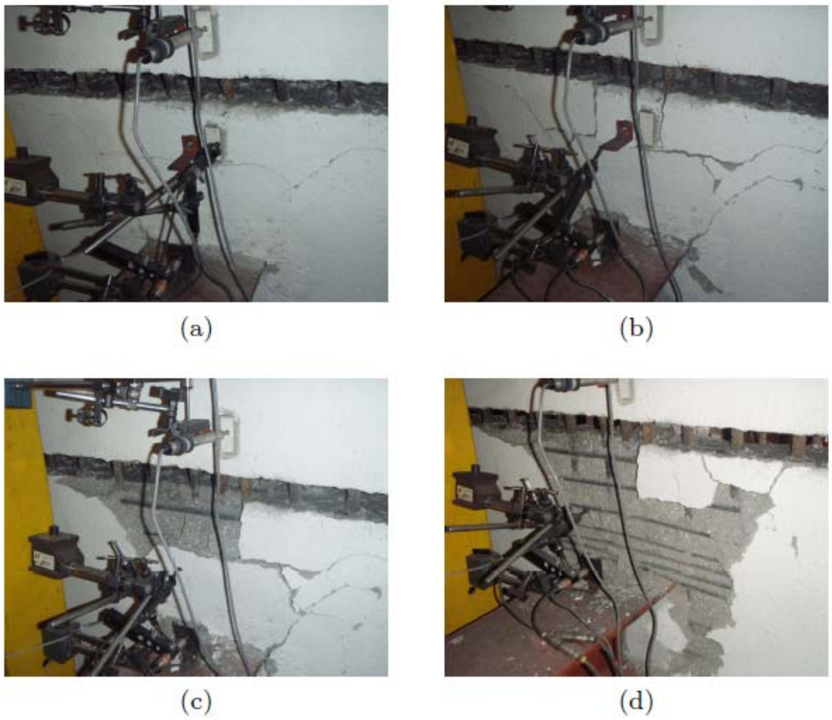

Fig. 14 Damage to the slab after: 2 tests (a), 4 tests (b), 5 tests (c) and 10 tests (d)

pinching phenomenon (and also, to a lesser extent, to the differences in strength), which directly affects the energy dissipation capacity. Pinching is a constriction of the moment-rotation diagram, contributing to a deviation from an elastic-perfectly plastic (EPP) behavior and resulting in a decreased energy dissipation capacity

The evolution of the deterioration between tests may also be interpreted through energy considerations. For this, the total amount of dissipated energy relating to different fuse plates is compared at the end of the first and second tests of each fuse, as shown in Fig. 13. The chart shows that, with the exception of plate D, the first tests were able to reach higher levels of energy dissipation. This indicates that the deterioration of the irreplaceable parts, particularly the cracking on the upper surface of the concrete slab (Figs. 14(a)-(d)), influences, albeit slightly, the energy dissipation capacity.

The evolution of energy dissipation over the cycles may also provide an idea of the progression of accumulated damage during the tests. This aspect was studied by computing the dimensionless parameter η/η_0, where η is an energy ratio at the end of each cycle and η_0 is the same energy ratio at the end of the first plastic cycle. According to ECCS (1986), the energy ratio η_i at the end of a cycle i is given by Eq. (2)

$$\eta_i = \frac{W_i}{\Delta M_y(\Delta\theta_i - \Delta\theta_y)} \tag{2}$$

where W_i is the energy dissipated in cycle i, ΔM_y is the range of the yield moments, $\Delta\theta_i$ is the range

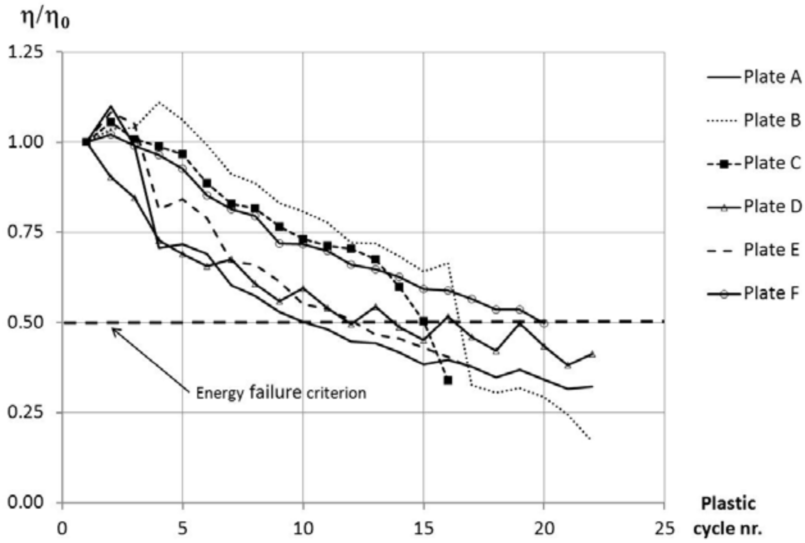

Fig. 15 Evolution of the energy dissipation ratio over the plastic cycles

of the imposed rotations at cycle i and $\Delta\theta_y$ is the range of the yield rotations. Fig. 15 shows the corresponding diagram for the first test of each specimen.

One possible energy failure criterion to be used consists of setting the η/η_0 parameter to a constant value that may depend on the geometric and material properties of the specimen, below which failure occurs. This criterion was used by Castiglioni and Pucinotti (2009) and Agatino (1995) to model the failure of steel components. As initially proposed by Calado and Castiglioni (1996), a simplified approach is to set the parameter to a constant value of 0.5. This limit appears in the diagram as the dashed line curve, which seems to fit adequately the experimental results, especially for fuse plates with a higher value of α. The same diagram also shows that the curves of fuse plates A and D cross this limit earlier in the test, with reference to their first plastic cycle. The corresponding plates tend to buckle more easily, therefore showing a more pronounced pinching effect.

In general, the results showed that fuses with higher values of α provide higher performance levels in terms of stiffness, resistance, dissipated energy and rate of deterioration. Nevertheless, fuses with values of α close to unity, and therefore whose strength is similar to that of the composite beam, induce more damage outside the fuse and thus fail to concentrate plasticity within the fuse section. This behavior contradicts one of the underlying concepts of the fuses and therefore the value of α should be limited by an upper bound to prevent plasticity from spreading into the irreplaceable parts.

4. Numerical modelling

4.1 Modelling assumptions

A set of six numerical finite element models – one for each flange plate type, A to F – were developed in Abaqus with the objective of reproducing the experimental results. These models were initially calibrated based on the experimental results, assuming that both the beam and column had a rigid behavior and that the composite beam presented full shear connection. Since the behavior of the fuse is mainly dependent on the yielding and buckling of the steel plates and no major cracking was observed in the first tests, concrete was modeled with an elastic behavior, thus considerably reducing the computational costs (Espinha 2011). The uniaxial stress-strain relationship adopted for steel was based on the results provided by experimental tensile tests carried out on samples taken from the steel profiles. These tests indicate that structural steel conforms to class S275 and the rebars to A500 grade. The properties of the steel were modeled with linear hardening and the Von Mises yield criterion was used, bearing in mind the provisions in EN 1993-1-1 and EN 1993-1-5 (CEN 2004).

4.2 Analysis of results

The validation of the numerical models was qualitatively conducted through the analysis of the deformed shapes and of the fuse moment-rotation relationships, considering the experimental results as a reference.


(a)

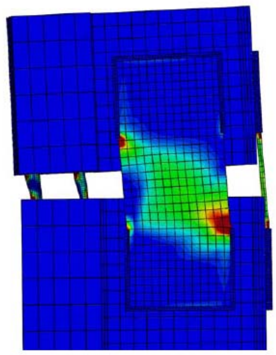
(b)

Fig. 16 Comparison between experimental (a) and numerical (b) deformed shape for sagging


(a)

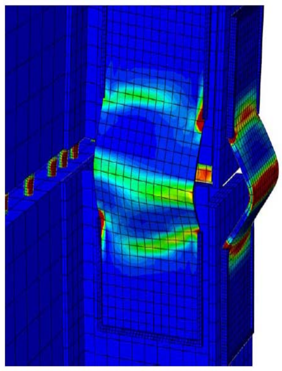
(b)

Fig. 17 Comparison between experimental (a) and numerical (b) deformed shape for hogging

The initial qualitative confrontation of the numerical model deformed shape with that of the experimental model can be exemplified for a single specimen, as displayed in Figs. 16(a)-(b) for sagging and Figs. 17(a)-(b) for hogging.

The former images represent the plastic deformation of the fuse in terms of the equivalent plastic strain contour plot. These plots show that the fuse was able to concentrate plasticity within the fuse plates, and also that some of the most relevant aspects of the experimentally-observed behavior, web and flange plate buckling patterns, are also conveniently reproduced by the numerical model.

The numerical simulations consisted of displacement-controlled increasing loading (monotonic) history, enabling qualitative comparisons with the experimental cyclic envelopes. An example of these comparisons is shown in Fig. 18.

In general, the models could predict the experimental behavior with relative accuracy, showing a good fit, especially under the elastic range. Taking the shape of both curves, it becomes clear that the yield properties of the numerical simulations for both hogging and sagging rotations agree with the experimental results. But in terms of the maximum moment, a more pronounced hardening is observed in the numerical model. Since the finite element model is loaded monotonically from the undeformed and undamaged condition, there is no deterioration from previous cycles that might have induced such resistance loss in the experimental tests, in particular for sagging rotations.

As far as the stiffness is concerned, the finite element model is stiffer than the tested experimental models. This difference is more marked for plates C, E and F, which were among the last to be tested experimentally. The difference could therefore be a consequence of the elastic stiffness loss shown by those specimens, due to the damage accumulation in the irreplaceable parts and also to cracking of the concrete and other low cycle fatigue effects.

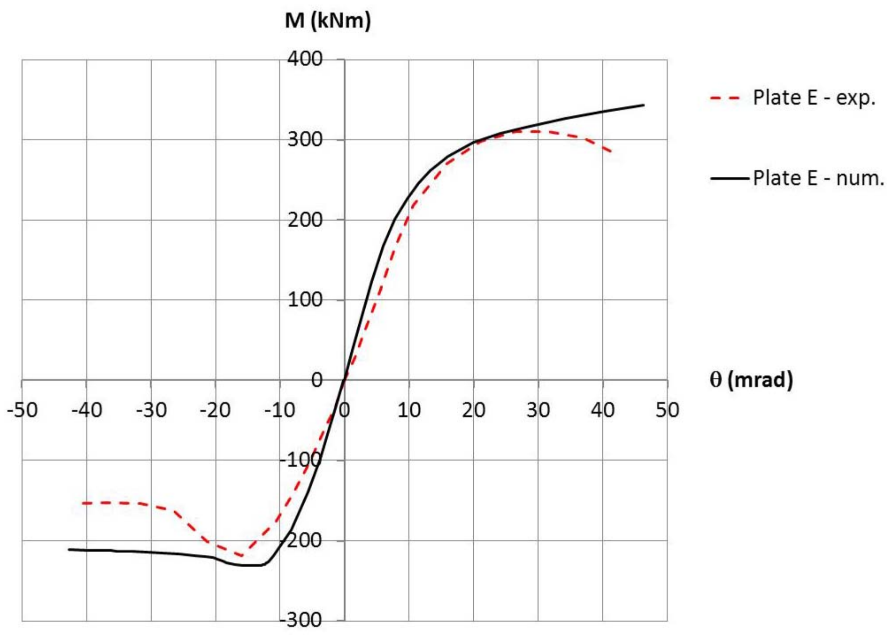

Fig. 18 Comparison between experimental and numerical results (fuse plate E)

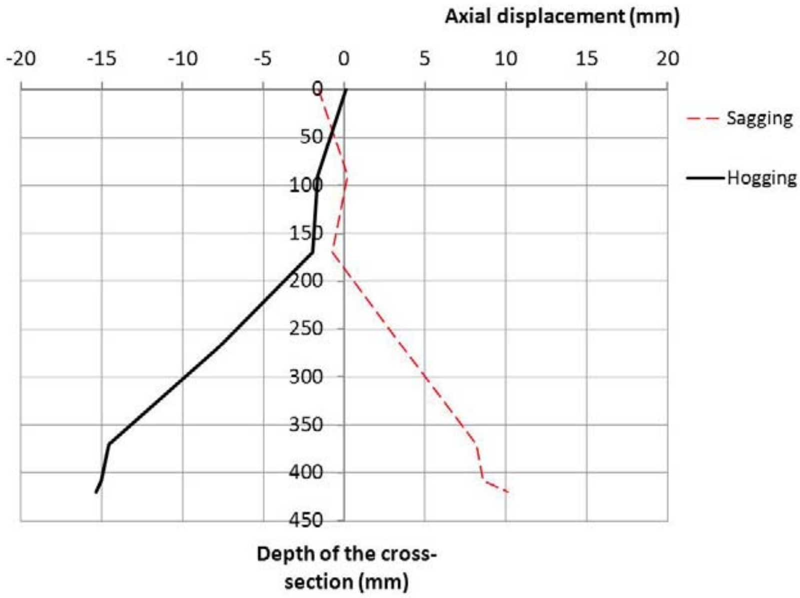

Fig. 19 Axial displacements through the depth of the cross-section of the fuse

Another aspect noted in the numerical results was that despite the fact that the plastic neutral axes lay close to the center of gravity of the rebar layers, the sections did not remain plane and, therefore, Bernoulli's hypothesis was not entirely valid. This conclusion is bound to create additional difficulties for the subsequent development of design models. The same conclusion can be inferred from the typical diagram of the axial displacements through the depth of the cross-section of the fuse, as shown in Fig. 19 for fuse C at maximum sagging and hogging rotations. It should here be stated that there were already some indications that the fuse region did not conform to the plane section hypothesis when analyzing the experimental readings of the dense array of displacement transducers placed in the same region.

5. Development of design models and comparison of results

To allow a simplified calculation of the main properties of the fuse, two separate design models were developed: a resistance and a stiffness model.

The design models were validated through the computation of the resistance and stiffness values for all fuses (based on the experimentally measured material properties) and subsequent comparison with the same quantities for the experimental tests.

5.1 Resistance model

The web plates of the fuse are fundamentally conceived to resist shear stresses. As a general rule these plates should present a cross-section greater than that of the web of the steel profile. Bearing in mind that shear may lead to brittle failure modes, bending-shear interaction could be detrimental to the bending resistance and ductility of the fuse. Therefore, and with respect to a plastic analysis, the contribution of the web plates to bending resistance may be neglected since they are mainly subjected to shear stresses. This assumption can be corroborated by the observation of the experimental deformation of the web plates since these are highly deformed and lie relatively close to the neutral axis. The same assumption leads to the simplified model for the computation of the resistance of the fuse cross section ($M_{\max,\, fuse}$) schematically represented in Fig. 20 ($R_{rebar,\, upper}$ and $R_{rebar,lower}$ represent the force in the two rebar layers, and R_{flange} the force at the flange plate).

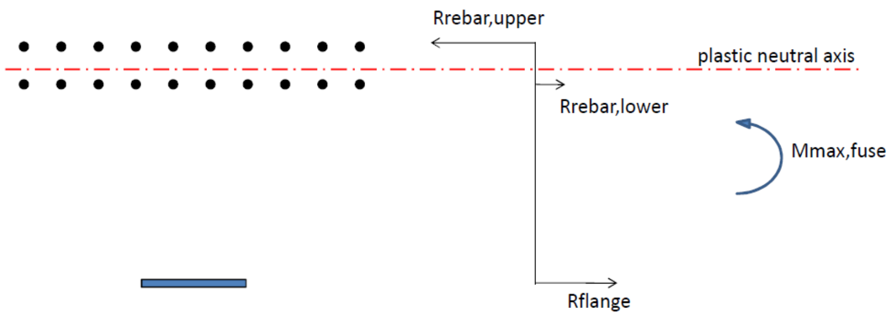

Fig. 20 Resistant cross section of the fuse design model

In spite of the fact that the plane cross section hypothesis does not entirely hold true, the resisting moment may be computed approximately by performing an elastic-plastic analysis with a single curvature, also neglecting the slip at the slab-beam interface. This model depends on the uniaxial $\sigma-\varepsilon$ constitutive relationships for all the materials involved. For the flange plate in compression, however, the real $\sigma-\varepsilon$ tensile curve had to be modified to account for the buckling phenomenon. In order to do so, a buckling model had to be developed based on the plastic mechanism of the plate at buckling, which is shown in Fig. 21.

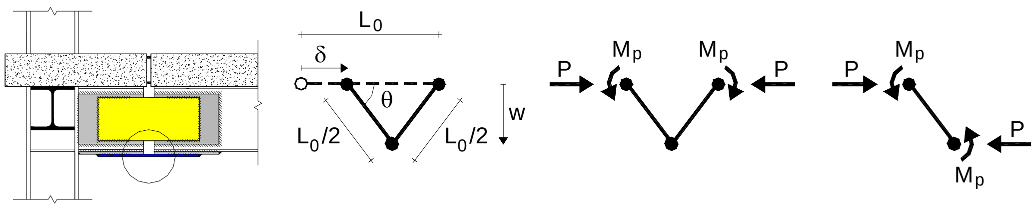

Fig. 21 Plastic mechanism of the fuse plates

The model is based on a previously developed model by Gomes and Appleton (1997) in which the elastic-plastic compression branch (yielding in compression) is limited by a buckling asymptote defined by Eq. (3)

$$\sigma_b = \frac{2\sqrt{2}M_p}{A\,L_0}\frac{1}{\sqrt{s}} \tag{3}$$

where σ_b is the stress with the buckling effect, M_p is the plastic moment of the cross-section of the flange plate, A is the cross-sectional area of the flange plate, L_0 is the free-length between the welds where the plate is not prevented from buckling, δ is the relative axial displacement between the two fixed points of the plate, ε is the equivalent average strain and P is the axial load. The hyperbolic $\sigma - \varepsilon$ buckling asymptote proposed by Gomes and Appleton was physically derived based on the plastic analysis of a compressed steel bar, considering the buckling length (here taken equal to the free length of the flange plates). The stress σ_c at compression is, for each strain, the lower absolute value of the stress at tension σ_t and the buckling stress σ_b.

Both the sagging and hogging maximum moments of the fuse were computed with the average constitutive relations of the materials obtained experimentally, with the aid of a MatLab code developed for this purpose. The computed sagging and hogging design moments are shown in Tables 4 and 5, respectively, in comparison with those measured in the experimental tests. The maximum moments computed by the numerical models are also shown for illustrative purposes. Only results from the first test of each specimen are compared, since the design model does not consider the deterioration effects arising from previous tests.

Design moment estimations seem to provide relatively adequate results regarding the expected level of accuracy. The nature of the errors is mainly related to the simplifying assumptions of the design model, such as the assumption that plane sections remain plane and that the total deformable length is equal to the free buckling length of the fuse. Figures for plates C, E and F showed less accurate results, overestimating the resistance at sagging, which could also be explained by the deterioration of the specimen assembly, which is more relevant in the specimens tested last.

Table 4 Comparison between maximum sagging moments results (in kNm)

	M^{+}_{exp}	M^{+}_{des}	Error$_{des\text{-}exp}$ (%)	M^{+}_{num}	Error$_{num\text{-}exp}$ (%)
A	250.7	259.0	+3.3	275.2	+9.8
B	294.4	338.5	+15.0	307.9	+4.6
C	286.5	341.7	+19.3	308.0	+7.5
D	247.6	257.5	+4.0	266.9	+7.8
E	314.5	418.9	+33.2	335.4	+6.6
F	273.2	309.5	+13.3	294.2	+7.7

Table 5 Comparison between maximum hogging moments results (in kNm)

	M^{+}_{exp}	M^{+}_{des}	Error$_{exp\text{-}des}$ (%)	M^{+}_{num}	Error$_{exp\text{-}num}$ (%)
A	-139.2	-147.2	+5.7	-161.9	+16.3
B	-174.7	-161.5	-7.6	-175.0	+0.2
C	-200.5	-162.1	-19.2	-196.1	-2.2
D	-124.6	-147.1	+18.1	-145.2	+16.5
E	-221.8	-175.6	-20.8	-230.7	-4.0
F	-130.8	-156.2	+19.4	-162.5	+24.2

In general, numerical models provided more accurate results than the design models, with errors below 10% in sagging. In hogging however, the numerical results showed increased, yet acceptable, errors.

5.2 Stiffness model

The design model developed aims at giving an approximate method of computing the initial stiffness of the fuses, $K_{fuse,ini}$ and is based on the component method of EN 1993-1-8 (CEN 2004). The proposed spring model is shown in Fig. 22.

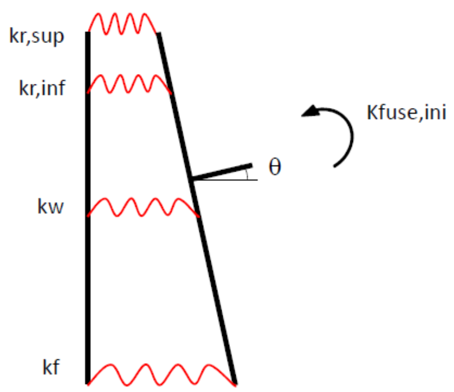

Fig. 22 Spring model of the fuse components

The four basic components identified are $k_{r.sup}$, $k_{r,inf}$, k_w and k_f, which correspond to the stiffness contribution of the upper rebar layer, lower rebar layer, web and flange plates, respectively. Contrary to the resistance model, the contribution of the web plates is accounted for in the stiffness model, since at low rotations these plates are not subjected to high shear stresses. Equation 4 was used to model the axial stiffness of the elements, which was also used by Hu *et al*. (2009) to compute the axial stiffness of the bolts in end-plate bolted connections.

$$k_{axial} = \frac{A}{L} \tag{4}$$

where A is the total area of the cross-section of the component and L is the free deformable length of the component. The deformable length of the rebar components was taken equal to the distance between transverse reinforcement (L = 100 mm) to account for some slip between the rebars and the adjoining concrete. The free deformable length for both the web and flange plates was set equal to the free length (170 mm) plus an extra length computed assuming a 45° degradation from the end of the welds.

Both the experimental tests and the numerical simulations have shown that the fuses may exhibit important shear deformations due to their flexibility. This effect was introduced in each of the components through an additional spring in series with the axial one, using the corresponding coefficients as defined in EN 1993-1-8 (CEN 2004).

The combination of the axial and shear deformability for each the components was performed assuming that the corresponding springs are assembled in series. The final stiffness of the fuse (considering the four components) was computed taking into consideration the final stiffness of each of the components and their location along the height of the fuse cross section.
The application of the proposed design model according to the provisions of EN 1993-1-8 (CEN 1994) gave the initial stiffness values of the fuse $K_{fuse,ini}$ presented in Table 6. These are compared with the initial stiffness values provided by the numerical model and by the experimental results from the first test on each specimen for sagging rotations.

Table 6 Comparison between stiffness results (in kNm/mrad)

	K_{exp}	K_{des}	K_{num}	$\mathrm{error}_{\mathrm{des\text{-}num}}$ (%)
A	23.99	27.50	29.53	-6.9
B	25.51	35.91	30.46	+17.9
C	25.62	36.35	30.50	+19.2
D	29.61	27.43	27.87	-1.6
E	20.57	40.64	31.42	+29.3
F	23.17	32.83	30.12	+9.0

One should notice that the initial stiffness experimental values are significantly affected by the deterioration of the irreplaceable parts induced by previous tests. It may therefore be misleading to compare the experimental and the design values, since the latter are not affected by deterioration. The error column in Table 6 is therefore the relative error between the design and the numerical models, considering these as a reference.

When compared with results from the numerical models, the proposed design model generally overestimates the stiffness values. This overestimation trend seems to increase with the capacity ratio α, as may be seen from the considerable difference obtained for plate E.

The shortcomings of the proposed method for the computation of the design stiffness result from the simplifying hypotheses, amongst which is the Bernoulli plane section hypothesis which disregards the slip between the reinforced concrete slab and the steel profile.

6. Conclusions

The developed fuses proved to be easy to replace and showed good performance indicators in terms of ductility, stiffness, energy dissipation and resistance. The fuses successfully protected the majority of the irreplaceable parts, which generally remained in the elastic domain as intended, which was in turn achieved by concentrating the inelastic behavior in the fuse plates. These fuses also proved to be easy to manufacture, to assemble and to replace.

It was observed that the value of the capacity ratio α is of major importance to characterizing the behavior of the fuse since it has a fundamental influence on its performance. It can thus be concluded that fuses with higher capacity ratio values also exhibit higher bending resistance and higher energy dissipation capacity. However, the capacity ratio should be upper bounded, since fuses with high values of α lead to increased deterioration of the irreplaceable parts, which is undesirable in view of the intended plasticity concentration features of the fuse.

Buckling of the fuse plates in hogging proved to govern the hysteretic behavior of the fuse. In spite of the fact that the fuses showed a stable hysteretic behavior, buckling induced a marked loss of strength in hogging, which did not allow the plates to exploit their full hardening capabilities. Furthermore, the severe low cycle fatigue effects caused by buckling contributed to the stiffness degradation of the fuse specimens during each test, especially in hogging.

The experimental results and observations allowed the calibration of numerical and design models. Generally speaking, the numerical models could predict the structural behavior with relative accuracy, showing a good fit with the experimental curves, especially in the elastic range.

The proposed design models provided satisfactory results, particularly in light of the rather simplified assumptions and the desired accuracy. There was, however, a deviation in some of the structural parameters, especially in those provided by the stiffness model. The strength and stiffness characteristics of the fuse may be computed by two different proposed models that correspond to different phases of the fuse behavior: the stiffness model captures the initial behavior of the fuse (predominantly elastic), whereas the strength model corresponds to a much later phase, clearly in the plastic range.

Acknowledgements

The studies reported in this paper were conducted under the FUSEIS (Dissipative Devices for Seismic Resistant Steel Frames, reference RSFR-CT-2008-00032) research project, financed by the Research Fund for Coal and Steel, of the European Commission. The availability of all the involved organizations – NTUA (National Technical University of Athens, Greece), PMIL (Politecnico di Milano, Italy), RWTH (Institute for Steel Structures, Aachen University, Germany), IST/UTL (Instituto Superior Técnico, Portugal) and SIDENOR SA (Greece) – as well as the supervision of Professor Ioannis Vayas (NTUA, Greece) are also acknowledged with gratitude.

References

Adany, S., Calado, L. and Dunai, L. (2001), "Experimental study on the cyclic behaviour of bolted end-plate joints", *Steel Compos. Struct.*, *Int. J.*, **1**(1), 33-50.

Agatino, M.R. (1995), "Criteri di collasso e modelli di danneggiamento per dettagli strutturale in acciaio soggetti a carichi ciclici", MSc Thesis, Politecnico di Milano. (in Italian)

Bruneau, M., El-Bahey, S., Fujikura, S. and Keller, D. (2010), "Structural fuses and concrete-filled steel shapes for seismic- and multi-hazard resistant design", *Proceedings of the 2010 NZSEE Annual Technical Conferenc*e, Wellington, New Zealand, March.

Calado, L. and Castiglioni, C.A. (1996), "Steel beam-to-column connections under low-cycle fatigue: Experimental and numerical research", *Proceedings of 11th WCEE*, Acapulco, Mexico, August.

Castiglioni, C.A. and Pucinotti, R. (2009), "Failure criteria and cumulative damage models for steel components under cyclic loading", *J. Constr. Steel Res.*, **65**(4), 751-765.

Castiglioni, C.A., Kanyilmaz, A. and Calado, L. (2012), "Experimental analysis of seismic resistant composite steel frames with dissipative devices", *J. Constr. Steel Res.*, **76**(1), 1-12.

Chan, R.W.K., Albermani, F. and Williams, M.S. (2009), "Evaluation of yielding shear panel device for passive energy dissipation", *J. Constr. Steel Res.*, **65**(2), 260-268.

Dubina, D., Ciutina, A.L. and Stratan, A. (2002), "Cyclic tests on bolted steel double-sided beam-to-column joints", *Steel Compos. Struct.*, *Int. J.*, **2**(2), 147-160.

European Convention for Constructional Steelwork (ECCS) Technical Committee 13 (1986), *Recommended testing procedures for assessing the behaviour of structural steel elements under cyclic loads*, No. 45.

Comité Européen de Normalisation (CEN) EN 1993-1-1 (2004), *Eurocode 3: Design of steel structures - Part 1-1: General rules and rules for buildings*, Brussels, Belgium.

Comité Européen de Normalisation (CEN) EN 1993-1-5 (2004), *Eurocode 3: Design of steel structures - Part 1-5: Plated structural elements,* Brussels, Belgium.

Comité Européen de Normalisation (CEN) EN 1993-1-8 (2004), *Eurocode 3: Design of steel structures - Part 1-8: Design of joints*, Brussels, Belgium.

Comité Européen de Normalisation (CEN) EN 1998-1 (2004), *Eurocode 8: Design of structures for earthquake resistance - Part 1: General rules, seismic actions and rules for buildings*, Brussels, Belgium.

Engelhardt, M.D. and Sabol, T. (1997), "Seismic-resistant steel moment connections: Developments since the 1994 Northridge earthquake", *Prog. Struct. Eng. Mat.*, **1**(1), 68-77.

Espinha, M. (2011), "Hysteretic behaviour of dissipative welded devices for earthquake resistant steel frames", MSc Thesis, Instituto Superior Técnico, Technical University of Lisbon.

Gomes, A. and Appleton, J. (1997), "Nonlinear cyclic stress-strain relationship of reinforcing bars including buckling", *Eng. Struct.*, **19**(10), 822-826.

Hsu, H.-L., Juang, J.-L. and Chou, C.-H. (2011), "Experimental evaluation on the seismic performance of steel knee braced frame structures with energy dissipation mechanism", *Steel Compos. Struct., Int. J.*, **11**(1), 77-91.

Hu, Y., Davison, B., Burgess, I. and Plank, R. (2009), "Component modelling of flexible end-plate connections in fire", *Int. J. Steel Struct.*, **9**(1), 1-15.

Koetaka, Y., Chusilp, P., Zhang, Z., Ando, M., Suita, K., Inoue, K. and Uno, N. (2005), "Mechanical property of beam-to-column moment connection with hysteretic dampers for column weak axis", *Eng. Struct.*, **27**(1), 109-117.

Krawinkler, H. (2009), "Loading histories for cyclic tests in support of performance assessment of structural components", *Proceedings of the 3rd International Conference on Advances in Experimental Structural Engineering*, San Francisco, US, October.

Li, H.-N. and Li, G. (2007), "Experimental study of structure with "dual function" metallic dampers", *Eng. Struct.*, **29**(8), 1917-1928.

Mazza, I. and Pedrazzoli, F. (2008), "Numerical modeling for innovative type of seismic moment resistant frames with dissipative, easy replaceable, joints", MSc Thesis, Politecnico di Milano.

Mazzolani, F.M. (2000), *Moment Resistant Connections of Steel Frames in Seismic Areas: Design and Reliability*, E & FN Spon, London-New York.

Mele, E., Calado, L. and De Luca, A. (2001), "Cyclic behaviour of beam-to-column welded connections", *Steel Compos. Struct., Int. J.*, **1**(3), 323-330.

Oh, S.-H., Kim, Y.-J. and Ryu, H.-S. (2009), "Seismic performance of steel structures with slit dampers", *Eng. Struct.*, **31**(9), 1997-2008.

Pachoumis, D.T., Galoussis, E.G., Kalfas, C.N. and Efthimiou, I.Z. (2010), "Cyclic performance of steel moment-resisting connections with reduced beam sections – experimental analysis and finite element model simulation", *Eng. Struct.*, **32**(9), 2683-2692.

Plumier, A. (1990), "New design for safe structures in seismic zones", *Proceedings of the IABSE Symposium on Mixed Structures Including New Materials*, Brussels, Belgium, 431-436.

Plumier, A., Doneux, C., Castiglioni, C., Brescianini, J., Crespi, A., Dell'Anna, S., Lazzarotto, L., Calado, L., Ferreira, J., Feligioni, S., Bursi, O., Ferrario, F., Sommavilla, M., Vayas, I., Thanopoulos, P. and Demarco, T. (2004), *Two Innovations for Earthquake Resistant Design – The INERD Project, Final report of research program CECA-7210-PR-316, Publication Nr 22044, Office des Publications des Communautés Européennes, Luxembourg* Research Fund for Coal and Steel (RFCS).

Yu, Q.-S. K. and Uang, C.-M., (2001), "Effects of near fault loading and lateral bracing on the behavior of RBS moment connections", *Steel Compos. Struct., Int. J.*, **1**(1), 145-158.

CC